

# $^{16}\text{N}$ as a calibration source for Super-Kamiokande

The Super-Kamiokande Collaboration

E. Blaufuss<sup>m,1</sup>, G. Guillian<sup>n</sup>, Y. Fukuda<sup>a</sup>, S. Fukuda<sup>a</sup>,  
M. Ishitsuka<sup>a</sup>, Y. Itow<sup>a</sup>, T. Kajita<sup>a</sup>, J. Kameda<sup>a</sup>,  
K. Kaneyuki<sup>a</sup>, K. Kobayashi<sup>a</sup>, Y. Kobayashi<sup>a</sup>, Y. Koshio<sup>a</sup>,  
M. Miura<sup>a</sup>, S. Moriyama<sup>a</sup>, M. Nakahata<sup>a</sup>, S. Nakayama<sup>a</sup>,  
Y. Obayashi<sup>a</sup>, A. Okada<sup>a</sup>, K. Okumura<sup>a</sup>, N. Sakurai<sup>a</sup>,  
M. Shiozawa<sup>a</sup>, Y. Suzuki<sup>a</sup>, H. Takeuchi<sup>a</sup>, Y. Takeuchi<sup>a</sup>,  
T. Toshito<sup>a</sup>, Y. Totsuka<sup>a</sup>, S. Yamada<sup>a</sup>, M. Earl<sup>b</sup>, A. Habig<sup>b</sup>,  
E. Kearns<sup>b</sup>, M.D. Messier<sup>b</sup>, K. Scholberg<sup>b</sup>, J.L. Stone<sup>b</sup>,  
L.R. Sulak<sup>b</sup>, C.W. Walter<sup>b</sup>, M. Goldhaber<sup>c</sup>, T. Barszczak<sup>d</sup>,  
D. Casper<sup>d</sup>, W. Gajewski<sup>d</sup>, W.R. Kropp<sup>d</sup>, S. Mine<sup>d</sup>,  
L.R. Price<sup>d</sup>, M. Smy<sup>d</sup>, H.W. Sobel<sup>d</sup>, M.R. Vagins<sup>d</sup>,  
K.S. Ganezer<sup>e</sup>, W.E. Keig<sup>e</sup>, R.W. Ellsworth<sup>f</sup>, S. Tasaka<sup>g</sup>,  
A. Kibayashi<sup>h</sup>, J.G. Learned<sup>h</sup>, S. Matsuno<sup>h</sup>, D. Takemori<sup>h</sup>,  
Y. Hayato<sup>i</sup>, T. Ishii<sup>i</sup>, T. Kobayashi<sup>i</sup>, K. Nakamura<sup>i</sup>,  
Y. Oyama<sup>i</sup>, A. Sakai<sup>i</sup>, M. Sakuda<sup>i</sup>, O. Sasaki<sup>i</sup>, S. Echigo<sup>j</sup>,  
M. Kohama<sup>j</sup>, A.T. Suzuki<sup>j</sup>, T. Inagaki<sup>k</sup>, K. Nishikawa<sup>k</sup>,  
T.J. Haines<sup>l,d</sup>, B.K. Kim<sup>m</sup>, R. Sanford<sup>m</sup>, R. Svoboda<sup>m</sup>,  
M.L. Chen<sup>n</sup>, J.A. Goodman<sup>n</sup>, G.W. Sullivan<sup>n</sup>, J. Hill<sup>o</sup>,  
C.K. Jung<sup>o</sup>, K. Martens<sup>o</sup>, M. Malek<sup>o</sup>, C. Mauger<sup>o</sup>,  
C. McGrew<sup>o</sup>, E. Sharkey<sup>o</sup>, B. Viren<sup>o</sup>, C. Yanagisawa<sup>o</sup>,  
M. Kirisawa<sup>p</sup>, S. Inaba<sup>p</sup>, C. Mitsuda<sup>p</sup>, K. Miyano<sup>p</sup>,  
H. Okazawa<sup>p</sup>, C. Saji<sup>p</sup>, M. Takahashi<sup>p</sup>, M. Takahata<sup>p</sup>,  
Y. Nagashima<sup>q</sup>, K. Nitta<sup>q</sup>, M. Takita<sup>q</sup>, M. Yoshida<sup>q</sup>,  
S.B. Kim<sup>r</sup>, M. Etoh<sup>s</sup>, Y. Gando<sup>s</sup>, T. Hasegawa<sup>s</sup>, K. Inoue<sup>s</sup>,  
K. Ishihara<sup>s</sup>, T. Maruyama<sup>s</sup>, J. Shirai<sup>s</sup>, A. Suzuki<sup>s</sup>,  
M. Koshiha<sup>t</sup>, Y. Hatakeyama<sup>u</sup>, Y. Ichikawa<sup>u</sup>, M. Koike<sup>u</sup>,  
K. Nishijima<sup>u</sup>, H. Fujiyasu<sup>v</sup>, H. Ishino<sup>v,i</sup>, M. Morii<sup>v</sup>,  
Y. Watanabe<sup>v</sup>, U. Golebiewska<sup>w</sup>, D. Kielczewska<sup>w,d,2</sup>,

S.C. Boyd<sup>x</sup>, A.L. Stachyra<sup>x</sup>, R.J. Wilkes<sup>x</sup>, K.K. Young<sup>x</sup>

<sup>a</sup>*Institute for Cosmic Ray Research, University of Tokyo, Kashiwa, Chiba  
277-8582, Japan*

<sup>b</sup>*Department of Physics, Boston University, Boston, MA 02215, USA*

<sup>c</sup>*Physics Department, Brookhaven National Laboratory, Upton, NY 11973, USA*

<sup>d</sup>*Department of Physics and Astronomy, University of California, Irvine Irvine,  
CA 92697-4575, USA*

<sup>e</sup>*Department of Physics, California State University, Dominguez Hills, Carson,  
CA 90747, USA*

<sup>f</sup>*Department of Physics, George Mason University, Fairfax, VA 22030, US A*

<sup>g</sup>*Department of Physics, Gifu University, Gifu, Gifu 501-1193, Japan*

<sup>h</sup>*Department of Physics and Astronomy, University of Hawaii, Honolulu, HI  
96822, USA*

<sup>i</sup>*Institute of Particle and Nuclear Studies, High Energy Accelerator Research  
Organization (KEK), Tsukuba, Ibaraki 305-0801, Japan*

<sup>j</sup>*Department of Physics, Kobe University, Kobe, Hyogo 657-8501, Japan*

<sup>k</sup>*Department of Physics, Kyoto University, Kyoto 606-8502, Japan*

<sup>l</sup>*Physics Division, P-23, Los Alamos National Laboratory, Los Alamos, NM  
87544, USA*

<sup>m</sup>*Department of Physics and Astronomy, Louisiana State University, Baton  
Rouge, LA 70803, USA*

<sup>n</sup>*Department of Physics, University of Maryland, College Park, MD 20742, USA*

<sup>o</sup>*Department of Physics and Astronomy, State University of New York, Stony  
Brook, NY 11794-3800, USA*

<sup>p</sup>*Department of Physics, Niigata University, Niigata, Niigata 950-2181, Japan*

<sup>q</sup>*Department of Physics, Osaka University, Toyonaka, Osaka 560-0043, Japan*

<sup>r</sup>*Department of Physics, Seoul National University, Seoul 151-742, Korea*

<sup>s</sup>*Research Center for Neutrino Science, Tohoku University, Sendai, Miyagi  
980-8578, Japan*

<sup>t</sup>*The University of Tokyo, Tokyo 113-0033, Japan*

<sup>u</sup>*Department of Physics, Tokai University, Hiratsuka, Kanagawa 259-1292, Japan*

<sup>v</sup>*Department of Physics, Tokyo Institute for Technology, Meguro, Tokyo 152-8551,  
Japan*

<sup>w</sup>*Institute of Experimental Physics, Warsaw University, 00-681 Warsaw, Poland*

<sup>x</sup>*Department of Physics, University of Washington, Seattle, WA 98195-1560, USA*

---

**Abstract**

The decay of  $^{16}\text{N}$  is used to cross check the absolute energy scale calibration for solar neutrinos established by the electron linear accelerator (LINAC). A deuterium-tritium neutron generator was employed to create  $^{16}\text{N}$  via the (n,p) reaction on  $^{16}\text{O}$  in the water of the detector. This technique is isotropic and has different systematic uncertainties than the LINAC. The results from this high statistics data sample agree with the absolute energy scale of the LINAC to better than 1%. A natural source of  $^{16}\text{N}$  from the capture of  $\mu^-$  on  $^{16}\text{O}$ , which is collected as a background to the solar neutrino analysis, is also discussed.

*Key words:* Solar Neutrinos; Calibration; Super-Kamiokande  
PACS: 26.65.+t

---

## 1 Introduction

The deficit of neutrinos coming from the sun, known as the solar neutrino problem, has long been established by past experiments[1–4]. A global analysis of these experimental results suggests an energy dependent suppression in the flux of solar neutrinos[5]. This suppression, via neutrino oscillations[6], could produce spectral distortions in the measured solar neutrino spectrum. Super-Kamiokande is the first experiment in a new generation of neutrino observatories that set out to measure the spectrum of neutrinos from the sun[7–9].

Super-Kamiokande (SK), a water Cherenkov detector, is sensitive only to the high energy  $^8\text{B}$  and rare HEP neutrinos from the sun. Detection of lower energy neutrinos is impeded by the high energy threshold of a water detector. The recoil electrons resulting from the elastic scatter of these neutrinos are observed in SK, providing energy and directional information in real time. Since the angular resolution of the detector for electrons of these energies is limited by multiple Coulomb scattering, performing a kinematic reconstruction of the incident neutrino energy is precluded. The measured electron energy is a lower limit of the neutrino energy and the shape of the solar neutrino energy spectrum must be inferred from the measured recoil electron spectrum. This situation increases the sensitivity to errors in the absolute energy scale when making solar neutrino flux and spectrum measurements. To set the energy scale, an electron linear accelerator (LINAC) was installed at SK to inject electrons of known energies into the detector[10]. In order to cross check this

---

<sup>1</sup> Corresponding author: Louisiana State University, Department of Physics and Astronomy, Baton Rouge, LA 70803, USA, Tel: +1 225 388 1137, Fax: +1 225 338 5855, e-mail blaufuss@phys.lsu.edu

<sup>2</sup> Supported by the Polish Committee for Scientific Research Grant 2P03B05316

calibration, the decay of  $^{16}\text{N}$  is used. First, a portable neutron generator has been employed to obtain high statistics data samples of  $^{16}\text{N}$  at many positions in the detector to accurately check the absolute energy scale. Second, the rate of  $^{16}\text{N}$  from the capture of stopped  $\mu^-$  is measured as a check of the solar neutrino analysis tools.

## 2 Solar neutrinos in Super-Kamiokande

Super-Kamiokande is a water Cherenkov detector located in the Kamioka Mine in Gifu, Japan. The walls of the cylindrical detector are constructed from welded stainless steel plates, backed with concrete. The detector is divided into an inner and an outer detector (ID and OD respectively) by a stainless steel frame structure that serves as an optical barrier and a mounting point for all photomultiplier tubes (PMTs). Cherenkov light in the ID is collected by 11,146 inward facing 50 cm PMTs mounted uniformly on the wall, providing 40% photocathode coverage. In the OD, 1,885 20 cm PMTs monitor the 2.5 meter thick veto region. The veto is used to tag incoming particles and serves as a passive shield for gamma activity from the surrounding rock. The ID encloses 32,500 metric tons of water in a volume that is 36.2 m in height and 33.8 m in diameter. The fiducial volume for the solar neutrino analysis starts 2 m inward of the walls of the ID and contains 22,500 metric tons of water. The ID is accessible by a set of calibration ports 30 cm in diameter leading from the top of the tank directly to the ID.

Solar neutrinos measured in SK have energies that range from 5 to 18 MeV. At these energies, the recoil electron is limited to a few centimeters in range and the vertex position is found using the relative timing of hit PMTs, assuming all Cherenkov photons came from a single point. Once a vertex is reconstructed, the direction of the electron is determined using the characteristic shape of the emitted Cherenkov radiation. Since roughly 6 photoelectrons in total are collected per MeV of energy, very few PMTs will have more than one photoelectron and the number of hit PMTs is used as a measure of the energy. This number is corrected for PMT dark noise, absorption and scattering of Cherenkov photons, and geometrical acceptance of the PMTs, which depends on the reconstructed vertex position and direction in the detector. This corrected number of hit PMTs must be properly translated into energy and should be uniform in all directions and throughout the volume.

The LINAC calibration provides this translation from the corrected number of hit PMTs to total energy. The LINAC[10] is located 15 meters from the top of SK, inset into the rock wall of the cavern. The electron beam is directed in a beam pipe through 9 meters of rock shielding, across the top of the SK tank, and down into the water by a series of bending and focusing magnets.

The beam momentum is adjustable from 5 to 16 MeV, matching the range of energies of  $^8\text{B}$  solar neutrinos. The absolute energy of the beam is measured with a germanium detector. LINAC data taken at several different positions and energies are used to set the absolute energy scale of the Monte Carlo (MC) detector simulation. The MC extrapolates this calibration to the entire range of energies, over the entire volume, in all directions. The resulting absolute energy scale is thought to be known with better than 1% uncertainty. To be confident with such a precise measurement, a secondary check with a calibration source of comparable precision is desirable.

The LINAC calibration has limitations. The electrons are only moving in a downward direction when they exit the beam pipe, possibly introducing systematic errors due to direction dependences of the detector. The presence of the beam pipe in the tank while calibration data are taken is another limitation. While this is modeled in the simulation, it is still the largest source of systematic error for the calibration, especially at low energies. Additionally, the beam pipe and equipment associated with the LINAC calibration can only be operated at a restricted set of calibration ports, so the calibration must be extrapolated to the entire fiducial volume. Operating the LINAC also requires a great deal of manpower and results in significant detector down time.

The deuterium-tritium neutron generator (DTG) pulsed calibration source was built to address the limitations of the LINAC calibration system, while providing a cross check of the absolute energy scale. The DTG creates  $^{16}\text{N}$  by the (n,p) reaction on  $^{16}\text{O}$  in the water of the detector. The decay of  $^{16}\text{N}$ , with a Q value of 10.4 MeV, is dominated by an electron with a 4.3 MeV maximum energy coincident with a 6.1 MeV gamma ray and is well suited to check the absolute energy scale for the solar neutrino measurement. With a half life of 7.13 sec,  $^{16}\text{N}$  is created *in situ* by lowering the DTG into the detector on a computer-controlled crane. After firing, the DTG is withdrawn, leaving the produced  $^{16}\text{N}$  to decay removed from the presence of any calibration equipment.  $^{16}\text{N}$  decays isotropically, making direction dependence studies on the energy scale possible. The calibration system is designed to be portable, permitting operation at virtually any calibration port, and providing a more complete mapping of the position dependence of the energy scale. The DTG is also designed to be easy to operate, requiring less manpower and down time for setup and data taking. The SNO experiment uses a similar DTG, externally located to their detector, as a neutron activation source for calibration purposes[11].

An additional source of  $^{16}\text{N}$  used for calibration at SK is the capture of cosmic ray  $\mu^-$  on  $^{16}\text{O}$ . These events are collected as a natural background in the solar neutrino analysis. These events occur at a comparable rate to solar neutrinos, and comparing the measured event rate to the expected rate serves as a check of the solar neutrino signal extraction method. These events, although limited

in statistics, can also be used to check the absolute energy scale.

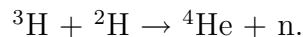
The following sections will describe the two methods by which  $^{16}\text{N}$  is produced for calibration in SK, including a description of the experimental setup used in taking DTG data, a discussion of  $^{16}\text{N}$  from the capture of  $\mu^-$ , as well as information regarding the simulation of the  $^{16}\text{N}$  beta decay. The results of the analysis of both data sets are also presented.

### 3 $^{16}\text{N}$ -Production and Modeling.

The  $^{16}\text{N}$  used as a calibration source for SK are produced by two different mechanisms. The first source results from the interaction of 14.2 MeV neutrons in the water of the detector. These neutrons are from a deuterium-tritium neutron generator (DTG), and produce a high statistics sample of  $^{16}\text{N}$  at a set position in the detector. The second source of  $^{16}\text{N}$  is the capture of stopped  $\mu^-$  in the water of the detector. These events, like solar neutrinos, are uniformly distributed throughout the detector volume. For both of these data sets, the beta decay of  $^{16}\text{N}$  is carefully modeled, and the corresponding MC is compared to the data. Since the energy scale of the MC is set by the LINAC calibration, a comparison of  $^{16}\text{N}$  data to MC serves as a cross check of the energy scale.

#### 3.1 $^{16}\text{N}$ from the DTG neutron generator

At the center of the DTG setup is a MF Physics Model A-211 pulsed neutron generator. This neutron generator creates neutrons by the deuterium-tritium reaction,



This reaction yields isotropically distributed neutrons with an energy of 14.2 MeV. The neutron generator consists of three main components, (1) an accelerator control unit, where high voltage ( $\sim 500$  V), operational interlock, and fire controls are located, (2) a pulse-forming electronics unit, where the  $\sim 100$  kV pulses needed by the accelerator are created, and (3) the accelerator head, containing the deuterium/tritium ion source and target. For operation at SK, where the separation between the accelerator control unit and the accelerator head could be up to 50 meters, the pulse-forming electronics were repackaged and attached directly to the accelerator head. The combined accelerator head and pulse electronics are encased in a stainless steel water-tight housing (Figure 1). The housing measures 150 cm in length and 16.5 cm in diameter,

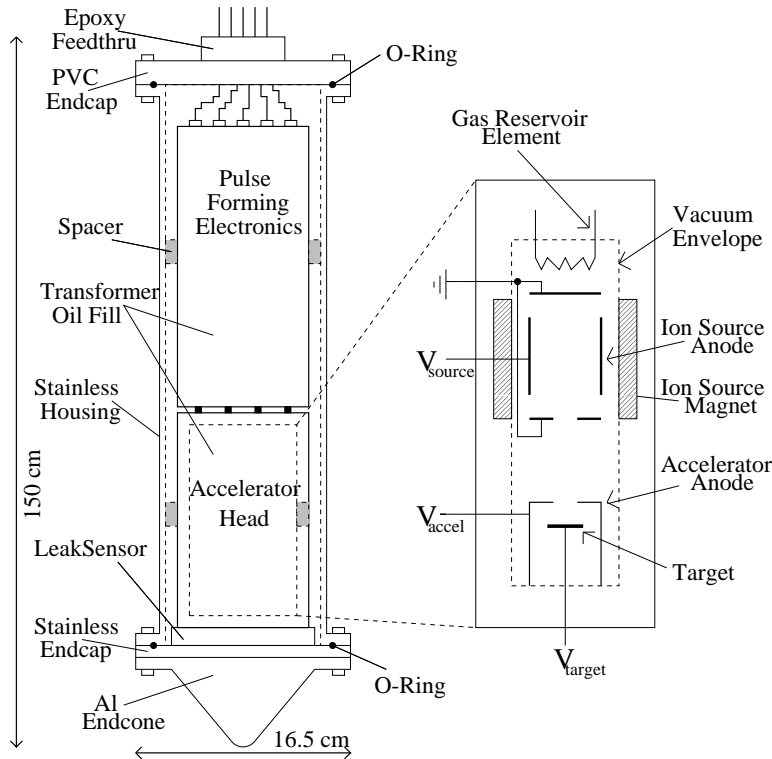


Fig. 1. Schematic of the DTG setup including the stainless steel water-tight housing, accelerator pulse-forming electronics and accelerator head. Details of the accelerator head are also shown.

fitting easily into the calibration ports at SK. The pulse-forming electronics are attached to the accelerator control unit by a cable bundle, containing 10 coaxial cables for high voltage and generator control signals. These cables pass through an epoxy filled cable feed-through on top of a PVC plate, which serves as the lid for the stainless steel housing. A water leak sensor is also included in the housing so that the generator can be removed in case of a water leak. An ultrasonic water sensor is also attached to the top of the steel housing and serves as an operational interlock, preventing operation of the generator when not in the detector. The entire DTG apparatus is moved into position in the detector using a custom built computer-controlled crane.

The DTG generates neutrons by colliding deuterium and tritium ions with a fixed metal hydride target, also containing equal parts of deuterium and tritium. These ions are created by a Penning ion source, using electric and magnetic fields to create a plasma along the source anode, and trapping the resulting electrons which ionize gas in the source region (see Figure 1). The gas pressure is regulated by the gas reservoir element. The deuterium and tritium ions are accelerated toward the target through an accelerating voltage of 80-180 kV. The target is biased positively with respect to the accelerating anode to prevent secondary electrons from damaging the ion source. The ion source, accelerating anode and target are enclosed in an evacuated enclosure,

which is in turn enclosed in a protective aluminum housing. The pulse-forming electronics are enclosed in a similar aluminum housing and both units are filled with Shell Diala AX transformer oil for insulation and cooling.<sup>3</sup> The neutron generator can be pulsed at a maximum rate of 100 Hz, with each pulse yielding approximately  $10^6$  neutrons.

The 14.2 MeV neutrons produced by the DTG are energetic enough to produce  $^{16}\text{N}$  by the (n,p) reaction on  $^{16}\text{O}$ [12] in the water of SK, which requires neutron energies greater than  $\sim 11$  MeV.[13]. The (n, $\alpha$ ) and (n,d) reactions on  $^{16}\text{O}$  result in the creation of stable isotopes, while the creation of  $^{15}\text{O}$  by the (n,2n) reaction is energetically forbidden. The (n,p) reaction on  $^{17}\text{O}$  and  $^{18}\text{O}$  are suppressed by the low isotopic abundance and smaller reaction cross sections, which results in yields  $< 1 \times 10^{-4}$  that of  $^{16}\text{N}$ . A simulation of neutrons in water using GCALOR and GEANT[14] indicates an expected  $^{16}\text{N}$  yield, defined as the fraction of neutrons that create  $^{16}\text{N}$ , of 1.3%. The actual yield of  $\sim 1\%$  found while taking data at SK agrees with this figure, given the uncertainties in the absolute neutron flux. These simulations also indicate that the mean distance these neutrons travel in water before they create  $^{16}\text{N}$  is about 20 cm.

When taking data at SK, the DTG is lowered to a position 2 meters above the intended  $^{16}\text{N}$  production point, and the data taking cycle is started (Figure 2). The data taking cycle is controlled by computer, directing the crane, the generator and data collection of SK. First, the crane lowers the DTG 2 meters, to the data collection position. Next, the generator is fired, creating a bubble of  $^{16}\text{N}$  surrounding the end of the DTG. Every time the DTG is fired, the generator is pulsed 3 times, at the maximum rate of 100 Hz, producing  $\sim 3$  million neutrons. Third, the DTG is raised 2 meters, removing the generator from the area containing  $^{16}\text{N}$ . After the DTG is fired,  $\sim 10$  seconds are required before the apparatus is completely withdrawn, and  $\sim 60\%$  of  $^{16}\text{N}$  has decayed. No data are collected while the crane is moving to prevent electrical noise generated by the crane from contaminating the data. Once the crane has stopped moving upward, data are collected in SK for 40 seconds. This cycle is repeated  $\sim 25$  times at a single location in the SK tank, yielding a data sample of  $\sim 300,000$   $^{16}\text{N}$  events collected by SK. This data sample is later analyzed using the standard analysis tools.

### 3.2 $^{16}\text{N}$ from the capture of $\mu^-$

The creation of  $^{16}\text{N}$  occurs naturally as a background to the solar neutrino measurement. A stopped  $\mu^-$  can be captured by a  $^{16}\text{O}$  nucleus in the water of the detector,

---

<sup>3</sup> The original fluorine-based insulating fluid was replaced with oil to remove contamination from  $^{16}\text{N}$  produced inside the generator from the (n, $\alpha$ ) reaction on  $^{19}\text{F}$ .

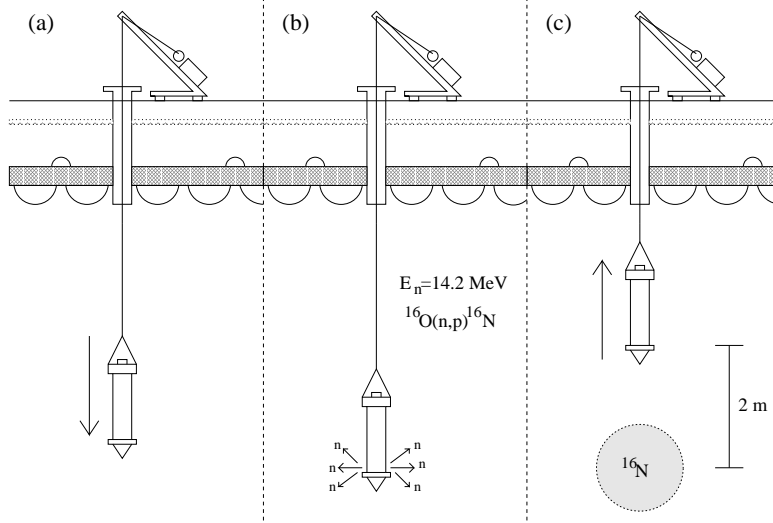
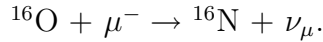


Fig. 2. An overview of DTG data taking. In (a), the DTG is lowered to the position where data is to be taken, The DTG is fired in (b) at that location, and (c) withdrawn 2 meters and data collected.



A fraction of  $^{16}\text{N}$  created will be in the ground state, and beta decays with a 7.13 sec half life. These events are found by collecting events that occur in the area surrounding the stopping point of a captured muon and subtracting random background events.

The expected rate of  $^{16}\text{N}$  events from muon capture per day in the inner 11.5 kton fiducial volume is given by

$$N_{ev} = N_{stop\mu} \left( \frac{\mu^-}{\mu^+ + \mu^-} \right) f_{capture} f_{gs} \epsilon,$$

where:

- $N_{stop\mu}$  is the rate of stopping muons found in the 11.5 kton volume per day. This rate is measured using the same stopping muon fitter that is used in the search for  $^{16}\text{N}$  events and is found to be  $2530 \pm 60(stat. + sys.)$  per day.
- $\left( \frac{\mu^-}{\mu^+ + \mu^-} \right)$  is the fraction of events that are  $\mu^-$ , taken to be  $0.44 \pm 0.01$ [18].
- $f_{capture}$  is the fraction of  $\mu^-$  that are captured on  $^{16}\text{O}$  before decaying, and is determined by the known capture and decay rates[19,20] to be  $18.39\% \pm 0.01\%$ .
- $f_{gs}$  is the fraction of captures that results in the formation of  $^{16}\text{N}$  in the ground state, where it will beta decay.  $f_{gs}$  is determined by the ratio of the partial capture rates to the ground state producing levels[16,21] to the total capture rate and is found to be  $9.0\% \pm 0.7\%$ .

Fraction	$J_i^p \rightarrow J_f^p$	$\Delta I$	Gamma Energy (MeV)	Type
66.2%	$2^- \rightarrow 3^-$	+1	6.129	GT allowed
28.0%	$2^- \rightarrow 0^+$	-2	none	GT 1st forbidden
4.8%	$2^- \rightarrow 1^-$	+1	7.116	GT allowed
1.06%	$2^- \rightarrow 2^-$	+0	8.872	F+GT allowed
0.012%	$2^- \rightarrow 0^+$	-2	6.049	GT 1st forbidden
0.0012%	$2^- \rightarrow 1^-$	+1	9.585	GT allowed

Table 1

Summary of information used in modeling the beta decay of  $^{16}\text{N}$ [17]. Gamma energies are also included. GT denote Gamow-Teller transitions and F denote Fermi transitions.

- $\epsilon$  is the triggering and reconstruction efficiency for  $^{16}\text{N}$  and is determined by MC simulation to be  $64.6\% \pm 0.2\%$ .

This results in a predicted  $^{16}\text{N}$  event rate in the 11.5 kton fiducial volume of  $11.9 \pm 1.0$  events per day. The inner 11.5 kton fiducial volume is chosen for the rate analysis to avoid contamination of the stopping muon sample from misidentification of through going muons near the walls of the detector. This contamination has no effect on the solar neutrino analysis.

### 3.3 Modeling the decay of $^{16}\text{N}$

Careful modeling of the  $^{16}\text{N}$  beta decay is crucial in order to perform accurate MC simulations of  $^{16}\text{N}$  data. All decay lines with a probability of  $10^{-8}$  or greater are included. Table 1 contains information about the included decay lines. In order to properly model the beta spectrum of these transitions, many corrections were applied[15]. These included corrections for nuclear recoil, the nuclear Coulomb field, finite nuclear size corrections, Dirac wave function corrections, radiative corrections and atomic screening. Additionally, the unique first forbidden transitions require corrections for the electron spectral shape[16]. These corrections tend to be significant only for very low energy electrons. In our case, individual corrections to the peak energy are all  $<0.2\%$ , and since they have different signs, the overall shift in the peak energy is only 0.14%. The electron and gamma energies obtained from this decay simulation are then input into the standard SK detector simulation used in the solar neutrino analysis.

## 4 Results from the DTG calibration

The DTG was installed at SK in March, 1999. The first few months of data taking were dedicated to engineering runs to optimize the data taking system and gain additional understanding of this new calibration data. Good, high statistics calibration data were obtained starting in July, 1999. At this time, a complete survey of the detector volume with the DTG was performed. Since that time, DTG calibration data have been collected monthly to monitor the long term stability of the energy scale. Results presented here are from the July 1999 detector DTG survey.

Data from the DTG are reconstructed using the same analysis tools as the solar neutrino analysis (see Reference [7]). No background subtraction is required when analyzing DTG data, as the natural background level contributes  $\ll 0.1\%$  to the data sample. The reconstructed vertex distributions for a typical data taking run are presented in Figure 3. Histograms of the x, y, and z vertices in SK coordinates are presented as well as x-z and y-z scatter plots. This data was taken at a nominal position of (-388.9 cm, -70.7 cm, 0 cm). The x and y vertex position are established by the position of the calibration port on the SK detector, and are accurate to  $\sim 3$  cm. The z vertex position is determined by the location of the crane, and since no effort was made during data taking to obtain the precise depth of the DTG, the z vertex position is accurate to  $\sim 25$  cm. The vertex distributions shown in Figure 3 have fitted peak positions from a Gaussian fit of (-389.2 cm, -72.8 cm, -27.8 cm). A small amount of smearing can be seen in the upper half of the z-vertex distribution resulting from water displaced by the withdrawal of the DTG. Given the spatial extent of the  $^{16}\text{N}$  created by the DTG, it is not the optimal tool for studies of vertex shifts or vertex resolution. For these studies, data from the LINAC is used. Reconstructed direction distributions are consistent with an isotropic source.

Monte Carlo data are generated at each position where data were taken. Reflection of Cherenkov photons from the DTG was included in the simulation, although geometric shadowing is expected for only 0.1% of photons. The data and MC events for a given position are subjected to the same reconstruction, and a histogram of the reconstructed energy is made for each. The energy spectrum from a typical data taking run is presented in Figure 4, along with the corresponding MC simulation. The peak of the energy distribution is dominated by events with a 6.1 MeV gamma ray in coincidence with an electron with a 4.3 MeV endpoint energy. 28% of the events contain an electron with an endpoint energy of 10.4 MeV and are the primary source of the observed high energy tail. The shape of the energy spectrum at low energies ( $< 5\text{MeV}$ ) is primarily determined by the trigger threshold of the detector. These distributions are fit with a Gaussian function between 5.5 MeV and 9.0 MeV, and the peak positions are found. These numbers serve as the measure of the ab-

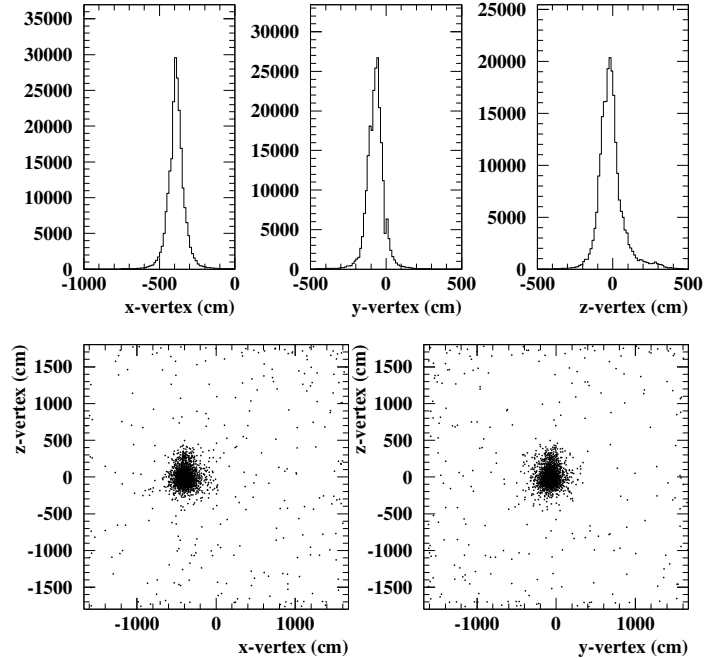


Fig. 3. Reconstructed vertex distributions for a typical data taking run. The x, y, and z-vertex position are in SK coordinates. SK uses a Cartesian coordinate system with the origin located at the center of the tank. This data was taken at  $(-388.9 \text{ cm}, -70.7 \text{ cm}, 0 \text{ cm})$ .

solute energy scale by calculating the deviation of peak positions,  $\frac{MC-DATA}{DATA}$ , and this procedure is repeated at each data position in the SK tank.

In order to obtain a global result from the deviation measured at various positions in the detector, a position-weighted average is performed on the results. Each position where DTG data are taken is given a weight based on the geometrical fraction the volume surrounding that point contributes to the total 22.5 kton fiducial volume. These weights vary from 1%-7% depending on the location in the detector. Since solar neutrinos interact uniformly throughout the entire detector volume, a position-weighted average provides a more realistic representation of the detector than a simple average. Figure 5 presents the position-weighted average energy spectrum for data and MC. There is excellent agreement between the two.

The data from the DTG are also used to study the position and direction dependence of the energy scale. DTG data was taken in 6 different calibration port locations, at 7 depths per port, providing a large sampling of the detector volume. The position dependence of the energy scale, shown in Figure 6, is presented as a function of radial distance ( $r$ ) and height ( $z$ ) in the detector, by performing a position-weighted average over  $z$  and  $r$ , respectively.

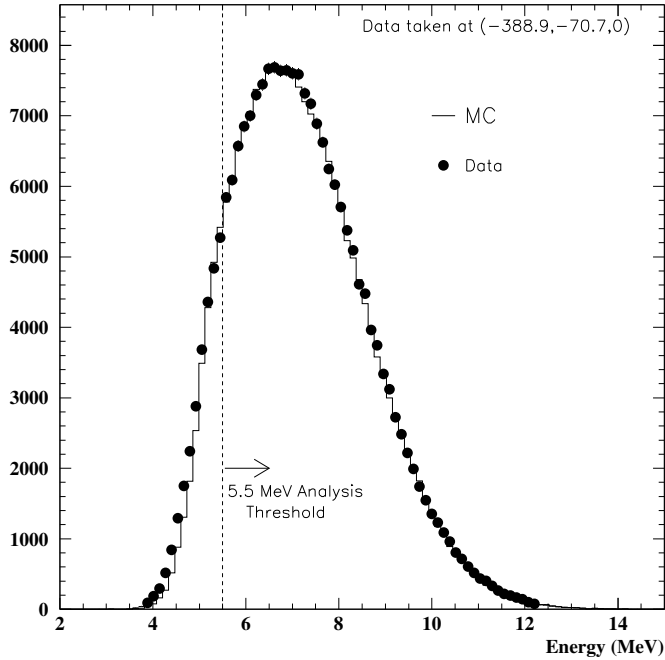


Fig. 4. Energy spectrum for Data and MC from a typical data taking run at a single point in the SK tank. The data (points) and MC (line) are fit with a Gaussian function only above the 5.5 MeV analysis threshold.

No significant variation in  $r$  is seen over the fiducial volume. While there is a slight variation with height in the detector, it is within the systematic errors for the energy scale. The direction dependence of the energy scale is obtained by dividing the data in subsets at each position based on the reconstructed direction, performing a Gaussian fit on the energy spectrum of each subset, and then performing a position-weighted average over all DTG data positions in the detector for each direction. The direction dependence is studied as a function of zenith angle, measured with respect to the vertical ( $z$ ) axis of the detector, and as a function of azimuthal angle, measured in the  $x$ - $y$  plane. The resulting angular dependence of the energy scale is presented in Figure 7. In both cases, the variation in the energy scale in direction within the fiducial volume is less than 1%.

As a check for background contamination from other nuclides, the half life of  $^{16}\text{N}$  is measured using the collected data. The time since generator fire for each event collected is plotted, and the data from several positions are combined for additional statistical weight. The histogram of this decay time and the calculated best fit are shown in Figure 8. The best fit half life of  $7.13 \pm 0.03$  sec is in excellent agreement with the expected value[17] of  $7.13 \pm 0.02$  sec, indicating a clean sample of  $^{16}\text{N}$  is obtained.

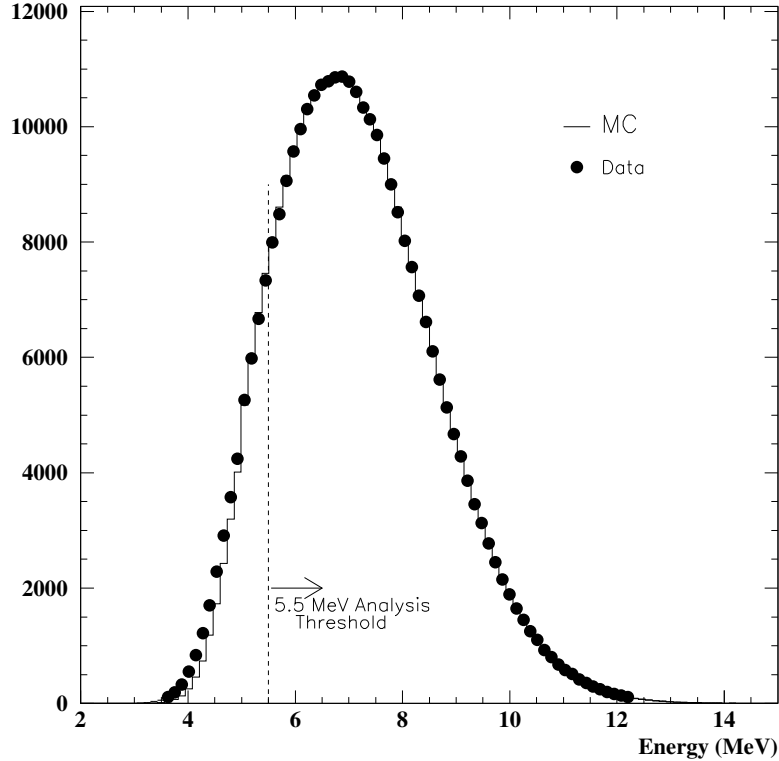


Fig. 5. The position-weighted average energy spectrum for data (points) and MC(line).

The systematic errors for the DTG calibration for the absolute energy scale measurement are summarized in Table 2. The systematic error for shadowing of Cherenkov photons by DTG related equipment after it is withdrawn is determined by the fraction of photons that could be absorbed and is conservatively estimated to be  $\pm 0.1\%$ . A simulation of neutrons in the DTG setup indicates that small amounts of background isotopes are created, including  $^{24}\text{Na}$ ,  $^{62}\text{Co}$ , and  $^{28}\text{Al}$ . Most nuclides have long half lives and/or insufficient energy to trigger SK, but a MC simulation indicates a small amount of gamma contamination is possible, and a systematic error of  $\pm 0.1\%$  is conservatively chosen. The DTG data selection systematic error results from a vertex position cut made to the data to remove background events occurring near the walls of the detector from the data sample.

The total position averaged energy scale deviation,  $(\frac{MC-DATA}{DATA})$ , measured during the July 1999 survey of the detector is found to be  $-0.04\% \pm 0.04\%(\text{stat.}) \pm 0.2\%(\text{sys.})$ , indicating excellent overall agreement of the DTG data with the LINAC-based MC simulation.

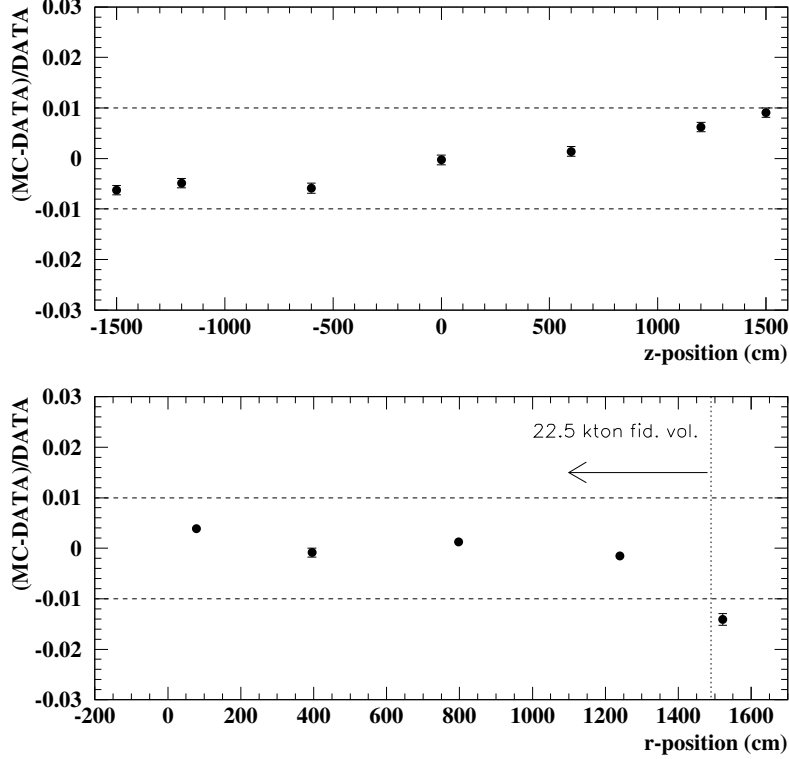


Fig. 6. Position dependence of the energy scale from DTG data. At each  $r$  and  $z$  vertex position, a position-weighted average over all  $z$  and  $r$  positions, respectively, is performed. Only statistical errors are shown. Dashed lines indicate a deviation of  $\pm 1\%$ .

Contamination from natural background	$< 0.01\%$
$^{16}\text{N}$ MC decay modeling	$\pm 0.1\%$
Unmodeled decay lines	$< 0.01\%$
Shadowing of Cherenkov photons	$\pm 0.1\%$
DTG data selection systematic	$\pm 0.1\%$
DTG related radioactive background	$\pm 0.05\%$
<b>Total Systematic Error</b>	<b><math>\pm 0.2\%</math></b>

Table 2

Summary of systematic errors from the DTG calibration.

## 5 Results from the $\mu^-$ Capture $^{16}\text{N}$ Analysis

$^{16}\text{N}$  data resulting from the capture of stopped  $\mu^-$  are simultaneously collected during normal data collection runs with solar neutrino events. In order to extract these few events per day from the data set, a specialized data search is implemented. First, stopping muon events are found and the stopping positions reconstructed. These fit results are used as an input, along with the input

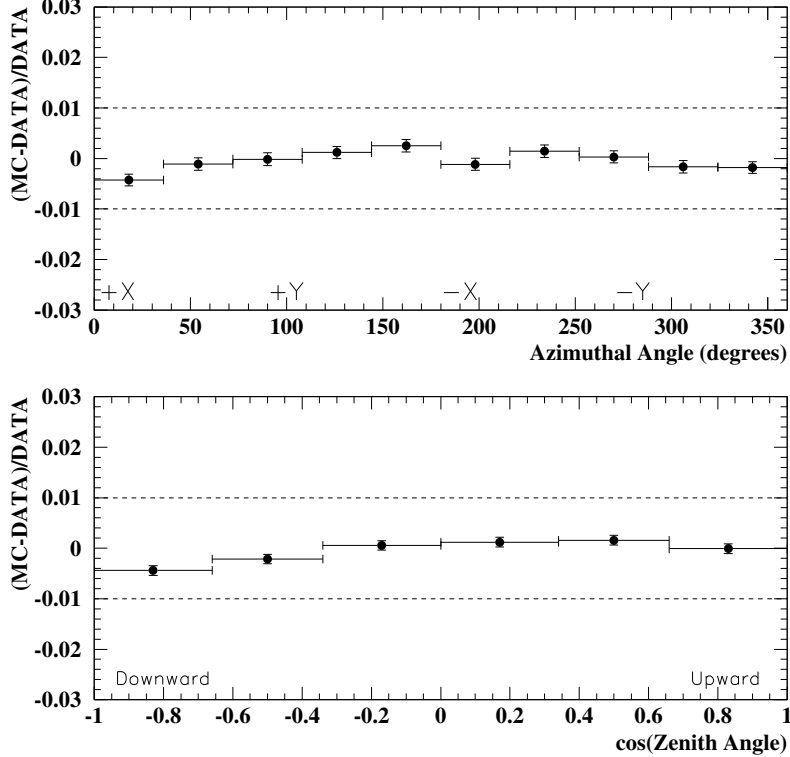


Fig. 7. Angular dependence of energy scale from DTG data obtained from a position-weighted average over all positions in the fiducial volume. An azimuthal angle of 0 degrees corresponds to the +X axis of SK. Only statistical errors are shown. Dashed lines indicate a deviation of  $\pm 1\%$ .

data for the solar neutrino analysis, to the  $^{16}\text{N}$  search program. The search program finds stopping muon events that are not followed by a decay event in  $100\mu\text{s}$ , as a muon that decays can not be captured on  $^{16}\text{O}$ , preventing additional background contributions. Once an “undecayed” muon is found, any events in the solar neutrino data sample are saved that occur within 335 cm of the stopping muon point, as well as in a time window of 100 ms to 30 seconds following the stopping muon. The distance of 335 cm is used as it is large enough to contain all expected signal events while keeping contributions from random backgrounds as small as possible. No limit is placed on the number of candidate signal events a stopping muon can produce to prevent biasing from the random background in SK. The result of this search is called the signal sample, and contains the  $^{16}\text{N}$  events as well as natural background events. To account for this natural background, a so-called background sample is also obtained by offsetting the times of the “undecayed” muons by 100 seconds into the future and again performing the same search.

Once the signal and background samples are compiled, the solar neutrino analysis algorithms are applied to all events. The effects of the natural background are removed by performing a statistical subtraction of the results for the background sample from the signal sample. In 1003.8 days of data, 41,059 signal

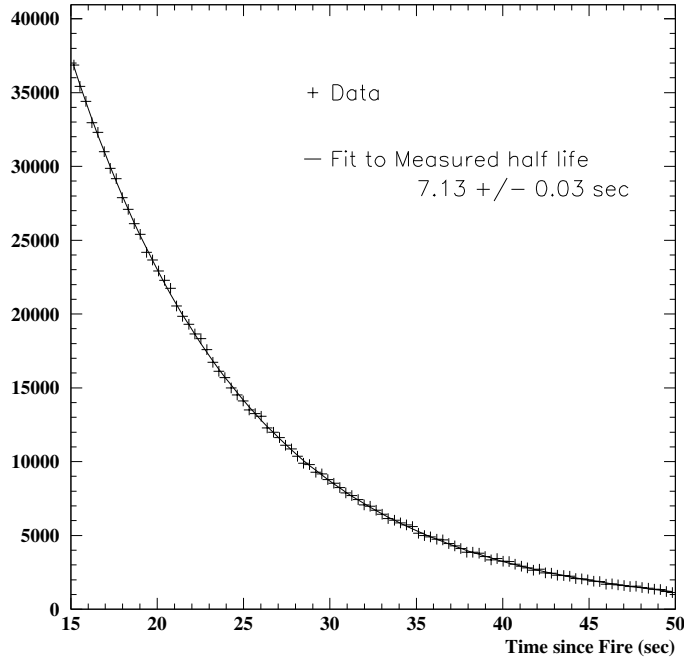


Fig. 8. Distribution of time since generator fire for several DTG runs. The data (crosses) and best fit (line) are shown. The expected half life is  $7.13 \pm 0.02$  sec. Data with time since fire less than 15 seconds are not shown to ensure all data is taken after the crane has been fully withdrawn.

sample events and 20,025 background sample events are found, resulting in an excess of 21,034 events attributed to  $^{16}\text{N}$  decay. In the inner 11.5 kton fiducial volume, 17,714 signal, with 6267 background events are found in this same live-time period, resulting in a rate of  $^{16}\text{N}$  events of  $11.4 \pm 0.2$  events/day. This result agrees well with the predicted rate of  $11.9 \pm 1.0$  events/day and indicates that no loss of signal is found for events in the same energy range of solar neutrinos.

These data are also used to check the absolute energy scale of the detector by comparing the energy distribution of the background subtracted sample to MC. A MC event sample is generated with measured decay electron positions used as input vertices. These events are reconstructed using the same tools as the signal and background samples. The background subtracted energy distribution is presented in Figure 9 along with the results from the MC. The fitted peak position for data and MC are found and compared, yielding a deviation ( $\frac{MC-DATA}{DATA}$ ) of  $+0.9\% \pm 0.7\%$ .

The background subtracted distribution of time since the stopping muon for  $^{16}\text{N}$  events is used to measure the half life, and is presented in Figure 10. The measured half life of  $6.68 \pm 0.14$  sec is in poor agreement with the expected

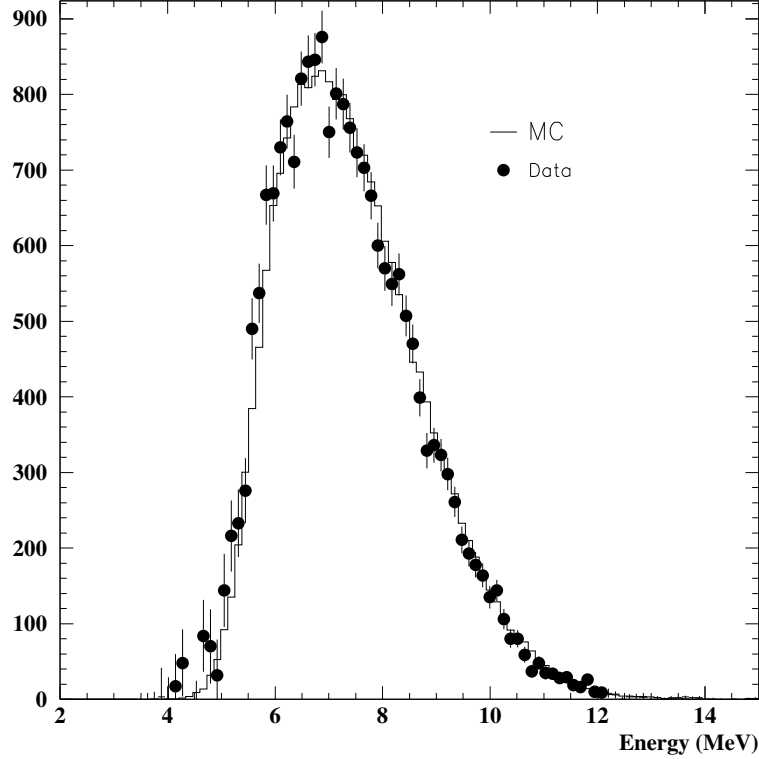


Fig. 9.  $^{16}\text{N}$  background subtracted energy distribution(points) along with MC expectations(line).

half life of  $7.13 \pm 0.02$  sec, with a 3.2 sigma difference. The poor agreement of the half life seems to indicate the presence of contamination in the data sample.  $^{15}\text{C}$  has been suggested, with a half life of 2.45 sec. It can be created by proton emission of some excited states of  $^{16}\text{N}$  formed during the capture of the  $\mu^-$ . Little is known about the highly excited states of the  $^{16}\text{N}$  nucleus[22], and this is taken as a systematic error for this analysis. The deviation of the measured half life from the accepted value can be interpreted as a  $\sim 4\%$  contamination from  $^{15}\text{C}$  and a MC of  $^{15}\text{C}$  decay events indicates that this would shift the energy distribution by  $-0.4\%$ . This type of contamination is not energetically possible for the DTG data sample. Additionally, the systematic error in modeling the decay of  $^{16}\text{N}$  from the DTG analysis also applies here, resulting in a total energy scale deviation for the  $\mu^-$  capture  $^{16}\text{N}$  of  $+0.9\% \pm 0.7\%$ (*stat.*) $^{+0.1\%}_{-0.5\%}$ (*sys.*)

## 6 Conclusions

The absolute energy scale of the Super-Kamiokande detector for solar neutrinos has been verified by the decay of  $^{16}\text{N}$ . In particular,  $^{16}\text{N}$  resulting from the (n,p) reaction of 14.2 MeV neutrons on water provides a high statistics data sample with comparable systematic uncertainties to the LINAC. Our analysis

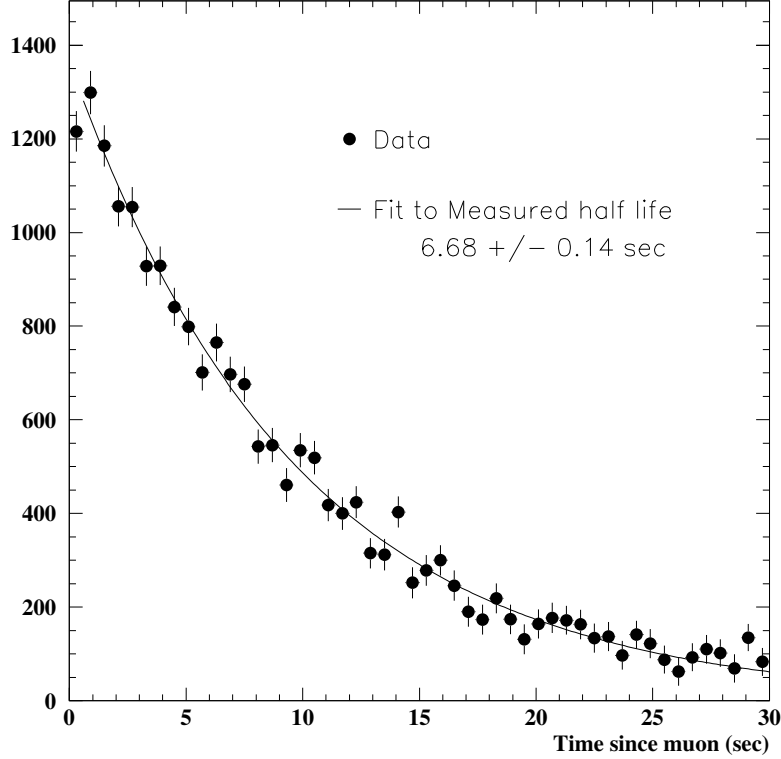


Fig. 10. Background subtracted distribution of time since stopping muon for  $^{16}\text{N}$  candidate events(points) and best fit to data(line).

shows excellent agreement (better than  $\pm 1\%$ ) between data and a LINAC-tuned MC simulation. The position and direction dependence of the energy scale have also been studied and are within our systematic uncertainties for the energy scale of the detector. The analysis of  $^{16}\text{N}$  events resulting from the capture of stopped  $\mu^-$  shows good agreement between the expected and measured rates of events and verifies solar neutrino flux measurements.

DTG data are periodically being collected to study the time dependence of the energy scale, and the DTG will continue to be used as a calibration tool for Super-Kamiokande. Future calibrations that combine the LINAC and DTG could result in smaller systematic uncertainties in the energy scale and more accurate measurements of the solar neutrino energy spectrum.

## 7 Acknowledgment

We gratefully acknowledge the cooperation of the Kamioka Mining and Smelting Company. This work was partly supported by the Japanese Ministry of Education, Science and Culture, the U.S. Department of Energy and the U.S. National Science Foundation.

## References

- [1] B. T. Cleveland et al., *Astrophys J.* **496** (1998) 505.
- [2] Y. Fukuda et al., *Phys. Rev. Lett.* **77** (1996) 1683.
- [3] J. N. Abdurashitov et al., *Phys. Rev. C* **60** (1999) 055801.
- [4] P. Anselmann et al., *Phys. Lett. B* **327** (1994) 377.
- [5] N. Hata, P. Langacker, *Phys. Rev. D* **56** (1997) 384.
- [6] S. P. Mikheyev, A. S. Smirnov, *Sov. J. Nucl. Phys.* **42** (1985) 913; L. Wolfenstein, *Phys. Rev. D* **17** (1978) 2369.
- [7] Y. Fukuda et al., *Phys. Rev. Lett.* **81** (1998) 1158.
- [8] Y. Fukuda et al., *Phys. Rev. Lett.* **82** (1999) 1810.
- [9] Y. Fukuda et al., *Phys Rev. Lett.* **82** (1999) 2430.
- [10] M. Nakahata et al., *Nuclear Instruments and Methods A* **421** (1999) 113.
- [11] J. Boger, et al., To be published in *Nuc. Inst. Meth. A*, nucl-ex/0010016.
- [12] W. Y. Chang, M. Goldhaber, R. Sagane, *Nature* **139** (1937) 962.
- [13] V. McLane, C.L. Dunford, P.F. Rose, *Neutron Cross Sections, Vol. 2* (Academic Press, Boston, 1982) 48.
- [14] GEANT Detector Description and Simulation Tool, *Cern Program Library W5013* (1994).
- [15] D.H. Wilkinson in *Nuclear Physics with heavy ions and mesons*, R. Balian et al., eds., (North Holland Publishing Co., 1978) 935.
- [16] M. Morita, *Beta Decay and Muon Capture* (W.A. Benjamin, Reading, MA, 1973) 32.
- [17] R. B. Firestone, *Table Of Isotopes, Vol. 1* (John Wiley and Sons, New York, 1996) 20.
- [18] S. Matsuno et al., *Phys. Rev. D* **29** (1984) 1.
- [19] C. Caso et al., *The European Physical Journal C* **3** (1998) 1.
- [20] T. Suzuki, D.F. Measday, and J.P. Roalsvig, *Phys Rev. C* **35** (1987) 2212.
- [21] P. Guichon et al., *Phys Rev. C* **19** (1979) 987.
- [22] D. R. Tiley, H. R. Walter, C. M. Cheves, *Nucl. Phys. A* **565** (1993) 1.